OXFORD

Cerebral Cortex, 2023, **33**, 5761–5773
https://doi.org/10.1093/cercor/bhac457
Advance access publication date 24 November 2022
Original Article

Functional reconfiguration of task-active frontoparietal control network facilitates abstract reasoning

Thomas M. Morin [1,2], Kylie N. Moore [1,2], Kylie Isenburg [1,2], Weida Ma[2], Chantal E. Stern[1,2,3,*]

[1]Graduate Program for Neuroscience, Boston University, 677 Beacon St., Boston, MA 02215, United States,
[2]Cognitive Neuroimaging Center, Boston University, 610 Commonwealth Ave., Boston, MA 02215, United States,
[3]Department of Psychological and Brain Sciences, 64 Cummington Mall, Boston University, Boston, MA 02215, United States

*Corresponding author: Kilachand Center for Integrated Life Sciences and Engineering, Boston University, Boston, MA 02215, United States. Email: chantal@bu.edu

While the brain's functional network architecture is largely conserved between resting and task states, small but significant changes in functional connectivity support complex cognition. In this study, we used a modified Raven's Progressive Matrices Task to examine symbolic and perceptual reasoning in human participants undergoing fMRI scanning. Previously, studies have focused predominantly on discrete symbolic versions of matrix reasoning, even though the first few trials of the Raven's Advanced Progressive Matrices task consist of continuous perceptual stimuli. Our analysis examined the activation patterns and functional reconfiguration of brain networks associated with resting state and both symbolic and perceptual reasoning. We found that frontoparietal networks, including the cognitive control and dorsal attention networks, were significantly activated during abstract reasoning. We determined that these same task-active regions exhibited flexibly-reconfigured functional connectivity when transitioning from resting state to the abstract reasoning task. Conversely, we showed that a stable network core of regions in default and somatomotor networks was maintained across both resting and task states. We propose that these regionally-specific changes in the functional connectivity of frontoparietal networks puts the brain in a "task-ready" state, facilitating efficient task-based activation.

Key words: fMRI; reasoning; functional connectivity; networks.

Introduction

Whether you are anticipating your opponent's next move in a chess match or finishing up a Sudoku puzzle on your morning commute, the human brain's remarkable reasoning capacity allows us to solve novel problems quickly by applying previously learned information, strategies, and ideas to new situations. Understanding how the human brain performs abstract reasoning tasks is a goal shared by neuroscientists studying cognition and engineers building brain-inspired artificial intelligence systems (Raudies and Hasselmo 2017; Hasselmo and Stern 2018; Do and Hasselmo 2021). Previous neuroimaging studies using matrix reasoning tasks have shown that increased activation of frontoparietal cortex supports abstract reasoning (Prabhakaran et al. 1997; Christoff et al. 2001; Kroger et al. 2002; Melrose et al. 2007, 2018; Golde et al. 2010; Shin and Jeon 2021). Evidence from human neuroimaging and computational modeling suggests that prefrontal cortex (PFC) in particular is essential for the more "abstract" portions of abstract reasoning, including representation and learning of specific rules (Hoshi et al. 2000; Wallis et al. 2001; Hasselmo and Stern 2018; Mansouri et al. 2020; Zhu et al. 2020) and deduction of the relationship between analogous stimuli (Bunge et al. 2005; Green et al. 2010; Watson and Chatterjee 2012). Moreover, anterior regions of PFC are activated more strongly as the relational complexity of a task (the number of rules that must be simultaneously considered) increases (Bunge et al. 2009; Cohen et al. 2018; Golde et al. 2010; Wendelken et al. 2012). This evidence supports theories of a hierarchical organization within the PFC, suggesting that more anterior regions of PFC represent and process more abstract information, such as the integration of multiple rules (Badre and D'Esposito, 2007, 2009; Badre and Nee 2018).

Studies of functional network connectivity have demonstrated that the functional reconfiguration of frontoparietal networks between resting and task states supports higher order cognitive functions such as abstract reasoning and cognitive control (Vakhtin et al. 2014; Hearne et al. 2015, 2017; Ray et al. 2020). Moreover, the frontoparietal control network supports the adaptive implementation of task-specific demands through flexible shifts in its global functional connectivity (Cole et al. 2013). In an earlier study using a matrix reasoning task, Hearne and colleagues demonstrated that increased functional connectivity between frontoparietal and visual cortices supported reasoning (2017). Moreover, the strength of this connectivity increased with relational complexity: as the number of rules being integrated increased, so did functional connectivity (Hearne et al. 2017). The Hearne et al. study showed a significant reconfiguration of functional connectivity with frontoparietal cortex between rest and task states, and relatively stable brain-wide connectivity during the task. Previous work from our lab shows that the formation of stable brain network community structures, particularly in somatomotor and ventral attention regions, also supports context-dependent rule learning (Morin et al. 2021). While previous work has identified regional task-related changes in functional connectivity, scores on tests of fluid intelligence are positively associated with increased overall similarity (reduced reconfiguration) in whole-brain task-based and resting-state functional connectivity (Schultz and Cole 2016; Ferguson et al. 2017; Hilger et al. 2020; Thiele et al. 2021).

Received: May 23, 2022. **Revised:** September 15, 2022. **Accepted:** October 27, 2022

In this study, we examined functional network reconfiguration using a simplified Raven's Progressive Matrices (RPM) task (Raven 1941). Our simplified RPM task was designed to test both symbolic and perceptual reasoning skills. Previously, studies have focused almost entirely on discrete symbolic versions of matrix reasoning, even though the first few trials of the Raven's Advanced Progressive Matrices task consist of continuous perceptual stimuli (Raven 1941). Specifically, we were interested in comparing activation related to synthesizing multiple discrete symbols (unique to the symbolic conditions) with activation related to identifying sequential patterns (present in all conditions).

Subjects in our study underwent fMRI scanning first during resting state, followed by the abstract reasoning tasks. Using a univariate approach, we examined the activity patterns that support perceptual and symbolic reasoning. We then characterized the functional network reconfiguration that occurred as subjects transitioned between resting state and the different task conditions. Based on existing literature, we predicted that our univariate results would demonstrate activation in frontoparietal cortex in support of both symbolic and perceptual reasoning (Golde et al. 2010; Melrose et al. 2007; Shin and Jeon 2021) and that prefrontal areas would activate more strongly for symbolic reasoning (Prabhakaran et al. 1997; Bunge et al. 2009), while inferior temporal areas would activate more strongly for perceptual reasoning (Sahyoun et al. 2010). At the network level, we predicted that a stable network core would be maintained across both resting state and the task conditions, with flexible reconfiguration of functional connectivity in frontoparietal regions supporting abstract reasoning (Hearne et al. 2017). Our results motivate a novel understanding of how the brain performs reasoning tasks: namely, nodes within frontoparietal cortex are functionally reconfigured, priming them to variably activate for unique task conditions.

Materials and methods

Participants

Thirty-one healthy participants with normal or corrected to normal vision and no history or current diagnosis of neurological or psychiatric disorders were recruited from Boston University and the greater Boston area for the current study. Twenty-seven participants were included in the final analysis (mean age 25.7 years; SD 3.57 years; range 19–34 years; 17 females, 10 males). One participant was excluded due to low accuracy on the behavioral task (<80% in at least one condition). Three participants were excluded due to excessive head motion (>3 mm head displacement during at least 2 TRs within a single run). All participants gave written informed consent in accordance with Boston University's Institutional Review Board and were compensated for their time.

Simplified Raven's progressive matrices task

During fMRI scanning, subjects performed a cognitive task designed to test their reasoning ability (see Fig. 1). In line with previous theoretical work, we defined reasoning as "the ability to take us beyond the confines of our current evidence or knowledge to novel conclusions about the unknown" (Sloman and Lagnado 2005). In practice, tasks that require more reasoning tend to take longer to solve. In addition to reasoning, dorsomedial and dorsolateral prefrontal cortex show activation related to time-on-task (Prabhakaran et al. 1997; Christoff et al. 2001; Kroger et al. 2002; Grinbrand et al. 2011; Gilbert et al. 2012). When designing the task for this study, we aimed to match time-on-task between reasoning and control conditions. With these controls in place, we can be more confident that activity in lateral prefrontal cortex is due to the introduction of reasoning demands in reasoning conditions, rather than other confounding time-based demands.

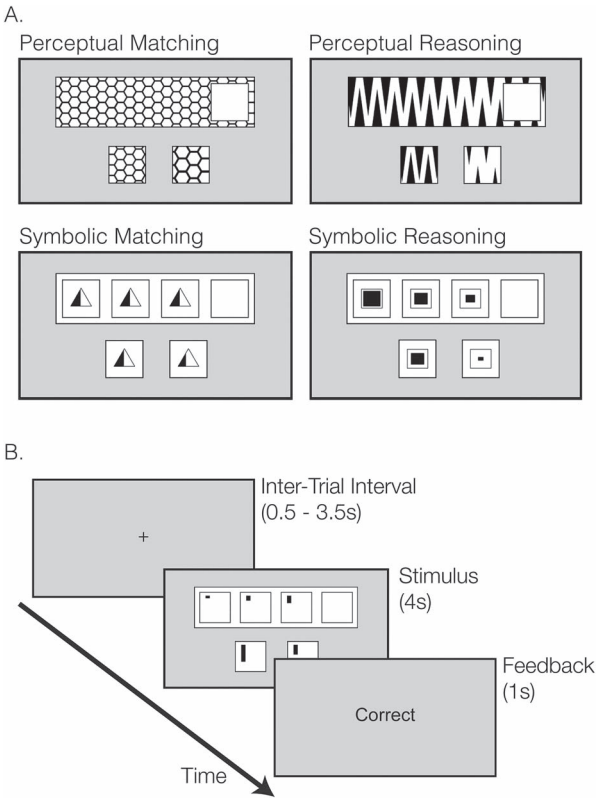

Fig. 1. Simplified Raven's progressive matrices task. A) During the task, subjects decided which of 2 answer choices best fit into the blank white square missing from the pattern at the top of the screen. A 2 × 2 task design was employed to test reasoning in two domains: symbolic and perceptual. Symbolic stimuli consisted of discrete squares each containing a symbol; perceptual stimuli consisted of continuous patterns. Reasoning stimuli progressed according to a pattern from left to right. As a control, matching conditions consisted of stimuli that were unchanging across the screen. B) During a single trial, subjects first viewed a fixation cross (0.5–3.5 s jitter). Next, they viewed the pattern and selected an answer choice with a button box (4.0 s). Finally, they were presented with feedback ("Correct," "Wrong," or "No Response") (1.0 s). Subjects completed 396 trials over the course of a 1-h fMRI scanning session divided into 6 task runs.

During each trial of the task, a stimulus with 2 answer choices appeared on the screen for 4.0 s and subjects indicated their response during this time by pressing the left or right button on a response-box. The stimulus and answer choices remained on the screen for the full 4.0 s time period, followed by 1.0 s feedback presentation period ("Correct," "Wrong," or "No Response"). Following feedback, a blank gray screen with a fixation cross appeared for a random jitter lasting between 0.5 and 3.5 s (values at 0.5 s intervals). The jitter was optimized to maintain orthogonality between conditions using the tool optseq2 available through Freesurfer (version 5.3.0) (Charlestown, Massachusetts; http://surfer.nmr.mgh.harvard.edu) (Fischl 2012).

Stimuli for the task were created with Adobe Illustrator (CS 5.1) and presented using PsychoPy (v1.90.3) (Peirce 2007, 2009). Stimuli consisted of simplified versions of the Raven's Standard Progressive Matrices (RPM) neuropsychological test (Raven 1941). To investigate the neural correlates of reasoning, we designed the task with four conditions: symbolic reasoning, symbolic matching, perceptual reasoning, and perceptual matching (see Fig. 1). In

the symbolic reasoning and perceptual reasoning conditions, the stimulus pattern varied from left to right according to a sequential rule, with discrete stimulus patterns in the symbolic reasoning condition and a continuous stimulus in the perceptual condition. Subjects were required to deduce and apply the sequence-rule to determine which of two answer choices correctly fit into a blank white square covering part of the stimulus. The symbolic matching and perceptual matching conditions were designed as control conditions to account for the visuospatial attention demands of the reasoning conditions. In the control conditions, there were no sequential rules for the stimuli, and the stimulus patterns were identical across the screen. Through behavioral piloting, task stimuli were specifically chosen so that response times would be matched across all 4 conditions and accuracy would be at ceiling. Our goal was to isolate brain signal due to abstract reasoning, and the reasoning conditions were paired with matching conditions that controlled for time-on-task, visual processing, and working memory demands.

The size of the pattern on the screen was matched across conditions. The blank white square could appear on either the left or right side of the pattern or sequence, and this was counterbalanced across trials and conditions. The location of the correct answer (left or right) was also counterbalanced across trials and conditions. Prior to scanning, the experimenter explained the task to the subject and guided them through eight sample trials using pen and paper. While in the MRI scanner, subjects completed 384 trials (96 in each of the four conditions). The experiment was divided into 6 runs, each lasting 6 min and 42 s. Conditions were counterbalanced within and across runs, and run order was randomized for each subject.

MRI data acquisition

Data was acquired on a 3 Tesla Siemens MAGNETOM Prisma magnetic resonance scanner located at the Boston University Cognitive Neuroimaging Center in Boston, Massachusetts. A 64-channel head coil was used for all scans. A T1-weighted MEMPRAGE RMS structural image was acquired for each subject [TR = 2200 ms, TE = 1.67 ms, Flip Angle = 7°, Voxel size = 1.0 mm isotropic] (van der Kouwe et al. 2008). Each subject underwent up to three runs of resting state fMRI (rs-fMRI) prior to task-based scans. During each rs-fMRI scan, subjects were asked to lie still with their eyes open for six minutes, while a fixation cross was displayed on the screen in front of them. For rs-fMRI scans, T2*-weighted echo-planar (BOLD) images were acquired using a multiband sequence (slice acceleration factor, 6) [TR = 1000 ms, TE = 30 ms, Flip Angle = 60°]. Twenty-four subjects underwent three consecutive six-minute resting state runs prior to completing the task scans. Due to time constraints, 3 subjects completed 2 resting state runs, and 1 subject completed one run. For task-based fMRI scans, T2*-weighted echo-planar (BOLD) images were acquired using a multiband sequence (slice acceleration factor, 3) [TR = 2000 ms, TE = 30 ms, Flip Angle = 60°, partial-Fourier acquisition]. For both the rest and task scans, a total of 78 slices were acquired, covering the whole brain. The simultaneous multislice (SMS)-EPI acquisition for resting state and task scans used the CMRR-MB pulse sequence from the University of Minnesota (Feinberg et al. 2010; Moeller et al. 2010; Setsompop et al. 2012; Xu et al. 2013; Cauley et al. 2014). Images were acquired with 2 mm isotropic voxels (matrix size 96 × 96) and the z-axis was aligned to the AC-PC line. Two opposite phase-encoded EPI fieldmaps (one anterior-to-posterior, the other posterior-to-anterior) were also acquired for each subject to be used for distortion correction of the functional images [TR = 8540 ms, TE = 66 ms, flip angle = 90°].

fMRI preprocessing

Both resting state and task fMRI data were preprocessed using a standardized pipeline available through fMRIprep (v1.4.1) (Esteban et al. 2019). Preprocessing steps included skull-stripping, distortion correction using magnetic field-maps, co-registration of each subject's functional data with their anatomical scan using boundary-based registration with 12-degrees of freedom, estimation of head-motion parameters, slice-time correction, spatial normalization of the subject's anatomical and functional data to standard template space (MNI152NLin2009cAsym template from templateflow), and projection onto a standardized cortical surface (fsaverage) (Ciric et al. 2021). Full details of the fMRIprep pipeline are outlined in the Supplementary Methods. After minimal preprocessing with fMRIprep, we performed spatial smoothing on the data (3 mm FWHM Gaussian kernel) using FSL (Zhang et al. 2001).

Univariate statistical analyses

Voxelwise analysis was performed on single subject data using a general linear model (GLM) implemented with AFNI's 3dDeconvolve command. GLM regressors included: a boxcar predictor function for each task condition (symbolic reasoning, symbolic matching, perceptual reasoning, and perceptual matching) spanning the 4 s period when the stimuli were displayed, a 3-degree polynomial (cubic) baseline term, six nuisance regressors per run for motion (x, y, and z translations and rotations), and four amplitude-modulated task regressors (one for each task condition) to account for signal related to response-time on each trial. Boxcar regressors were convolved with a standard hemodynamic response function (HRF). High motion time points (>0.5 mm frame-to-frame head movement or outlier fraction >0.1), as well as incorrect trials, were censored from the GLM analysis. Two-sided *t*-tests were conducted at each voxel to determine differences in activation between conditions using AFNI's 3dttest++ command. Group statistical maps were thresholded using AFNI's equitable thresholding and clustering (ETAC) method (Cox 2019). For visualization, we also included results projected onto inflated cortical surface maps (thresholded at $P < 0.05$, cluster size >20 vertices) (see Fig. 2).

Yeo-7 network ROI analysis

We examined differences in BOLD signal within functional brain network regions of interest (ROIs) as defined by the Yeo-7 functional network atlas available in Freesurfer (Yeo et al. 2011). The mean BOLD percent signal change in the perceptual and symbolic reasoning vs. matching contrasts was extracted from each Yeo-7 network ROI (visual, somatomotor, dorsal attention, ventral attention, limbic, cognitive control, and default) for each subject. The mean BOLD percent signal change was plotted as a bar-graph and results are displayed in Fig. 3. Error bars represent a 95% confidence interval based on between-subjects mean and variance. *T*-tests were conducted to determine which of the seven networks showed statistically significant changes in BOLD signal between the symbolic and perceptual conditions. Results were corrected for multiple comparisons using Bonferroni-correction.

Functional connectivity measures

Prior to calculating task and resting state functional connectivity measures, preprocessed data was further denoised using linear regression. All denoising and functional connectivity calculations were implemented in the CONN Toolbox

(Whitfield-Gabrieli and Nieto-Castanon 2012). In the denoising procedure, confound regressors included 6 head-motion parameters and their first-order temporal derivatives, linear drift, and 5 noise components from CSF and white matter ROIs (the mean signal as well as the first 4 components from a principal component analysis in each ROI) (Chai et al. 2012). High-motion time-points (>0.5 mm frame-to-frame head movement or outlier fraction >0.1) were censored as part of the denoising procedure. For the task-based scans, task-related signal from each of the 4 task conditions was also removed from the time series using HRF-convolved boxcar functions and their first-order derivatives. Regression of task-related signal is essential to ensure that functional connectivity observations were due to low-frequency coupling, rather than interregional similarities in task-based activation (Gonzalez-Castillo and Bandettini 2018; Tomasi and Volkow 2019). Finally, the denoised time series was band-pass filtered (0.008–0.09 Hz) to isolate the frequency-band of interest that is most commonly associated with BOLD signal.

For resting state scans, functional connectivity between two regions i and j was defined as the Fisher-Z transformed Pearson correlation between the ROI timeseries. For task scans, a weighted GLM was employed to first isolate the signal associated with each condition in our event-related design. Weights were constructed as condition-specific boxcar timeseries convolved with a canonical HRF. Pearson correlation was calculated between the condition-specific signal extracted from each pair of ROIs, followed by Fisher-Z transformation. For each subject, the result was a functional connectivity matrix A_{ij} (400×400 ROIs in size) for each of five conditions: resting state, symbolic reasoning, symbolic matching, perceptual reasoning, and perceptual matching.

Notably, the analysis approach we adopted was previously used by Hearne and colleagues to compare network organization at rest with network organization during an event-related task design (2017). Preprocessing and denoising procedures were identical across task and resting state data, except for regression of task-related signal in the task data, and bandpass filtering of resting-state data. Task-based functional connectivity was calculated using a weighted GLM approach that created condition-specific (weighted) time-series of fMRI data. This approach keeps the data in a similar format to the resting state data (namely a 4D series of BOLD-signal volumes) and improves our ability to compare functional connectivity metrics across rest and task.

Network reconfiguration analysis

We conducted a network reconfiguration analysis based on methods from Hearne et al. (2017). The goal of this analysis was to divide the functional connectivity network into communities and track community-membership changes across resting state and task conditions. A community is defined as a group of nodes that exhibit stronger connectivity to each other in the whole-brain network than they do in a relevant null model (Newman and Girvan 2004; Hearne et al. 2017). The five weighted connectivity matrices for each subject were thresholded so that only the top 20% of connections remained in the matrix. Because the threshold level can influence network statistics (Rubinov and Sporns 2011), we repeated all statistics at 5, 10, 15, 20, 25, and 30% thresholds. This ensured that when comparing different networks across subjects and conditions, differences in network statistics were not influenced by differing edge densities (Garrison et al. 2015). Varying the threshold did not result in any significant changes to the network measures described below, therefore we present results at the 20% threshold in the main text. See Supplementary Figs. S1 and S2 for results presented at each of the other thresholds.

The thresholded, weighted matrices were subjected to a Louvain community detection algorithm implemented in the Brain Connectivity Toolbox (Rubinov and Sporns 2010). The Louvain community detection algorithm generates community assignments that maximize the modularity, Q, which is defined as (Newman and Girvan 2004; Fortunato 2010):

$$Q(\gamma) = \frac{1}{2m}\sum_{ij}\left[A_{ij} - \gamma P_{ij}\right]\delta\left(\sigma_i\sigma_j\right),$$

where A_{ij} is the weighted and thresholded functional connectivity matrix, $2m$ is the sum of all the edge weights in the graph, $P_{ij} = \frac{k_i k_j}{2m}$ is the expected number of edges between nodes i and j according to a null model that preserves degree sequence of the graph, and $\delta(\sigma_i\sigma_j) = 1$ if the community assignment of node i is the same as the community assignment of node $j(\sigma_i = \sigma_j)$, and is zero otherwise. The resolution parameter γ determines the size of the final communities, with $\gamma < 1$ leading to larger communities and $\gamma > 1$ leading to smaller communities. In line with previous work, we fixed $\gamma = 1$.

Because the outcome of Louvain community detection is dependent on initial conditions (e.g. which node is first assigned to a community), we repeated this process 1,000 times for each connectivity matrix. To obtain a single set of community assignments for each subject and condition, we ran the following consensus procedure: first, an agreement matrix B was calculated in which each element B_{ij} represented the probability that 2 nodes were classified into the same community across all 1,000 iterations of Louvain community detection for a particular subject and condition. Then, we performed module-based consensus partitioning on the agreement matrix to obtain a single set of community assignments for each subject and condition. The entire consensus procedure was repeated across subjects to obtain a single set of community assignments per condition that was consistent across the entire group of subjects. The changing community memberships were plotted in an alluvial flow diagram (using the R packages *easyalluvial* and *parcats*) (Rosvall and Bergstrom 2010) (Fig. 4).

It is possible that network reconfiguration observed between the resting state and task conditions could be influenced by the different scanning parameters used to acquire resting state and task fMRI (resting state: TR = 1.0 s, slice acceleration = 6; task: TR = 2.0 s, slice acceleration = 3). To ensure that the network reconfiguration we observed was due to changes in functional connectivity rather than differences in scanning parameters, we conducted two follow-up analyses. Like the other analyses presented in the main text of this manuscript, these follow-up analyses were performed using functional connectivity matrices that were thresholded for the top 20% of connections. First, we tested whether a decrease in signal to noise ratio (SNR) during resting state scanning (due to the higher temporal resolution) may have resulted in a finer distinction among communities. To test for this, we analyzed the community structure of each of the three resting state runs separately. This first analysis included only the 23 subjects who completed all 3 resting state runs. Assuming a community partition is due to signal rather than noise, we should expect to see a similar community partition across all three resting state runs when they are analyzed separately. Second, we tested whether the increased temporal resolution of the resting state data (compared to task data)

may have resulted in a finer distinction among communities. To test for this, we downsampled the resting state fMRI data by averaging adjacent TRs, and repeated the network reconfiguration analysis on the downsampled data. To quantify differences in community partitions that were calculated during these follow-up analyses, we used the variation of information (V_{In}) statistic that is described below. Results from the 2 follow-up analyses are presented in Supplementary Fig. S3.

Finally, to demonstrate fluctuating activity levels within stable task communities, we extracted the mean BOLD signal from each consensus community during each of the four task conditions (Fig. 5C) (see Supplementary Fig. S2 for results plotted across edge threshold levels.) A repeated measures ANOVA with paired *T*-test post-hoc testing was conducted to assess which communities exhibited significantly different activity levels across conditions. Results were corrected for multiple comparisons using Bonferroni correction.

Statistical analysis of community structure

To evaluate the extent to which community structure changed between resting state and each task condition within subjects, we calculated the information theoretic distance (variation of information, V_{In}) between the consensus community assignments for each condition (Braun et al. 2015). V_{In} is defined as (Meilă 2007):

$$V_{In} = \frac{H(X) + H(Y) - 2\mathbf{MI}(X, Y)}{\log(n)},$$

where X and Y are vectors listing the community assignments of n nodes in two different conditions, H is the entropy, and **MI** is the mutual information.

To assess the significance of V_{In} measures, we followed the procedure outlined by Hearne et al. to generate a null distribution of V_{In}. Briefly, we generated 10,000 permutations of community assignments by randomly selecting half of the subjects to switch their condition labels (e.g. when comparing symbolic reasoning and resting state community assignments, the condition labels were switched for half of the subjects, and a new consensus community structure and V_{In} metric were computed and added to the null distribution).

To compare the extent to which individual communities exhibited change between resting state and the task conditions, V_{In} was also computed separately for each of the 3 task communities, repeated across all 4 task conditions. Results are plotted in Fig. 5b (see Supplementary Fig. S1 for results plotted across edge threshold levels). A repeated measures ANOVA was employed to determine whether there was a difference in V_{In} across task communities and/or task conditions. Results from paired *T*-test post hoc testing were corrected for multiple comparisons using Bonferroni correction.

Results

Behavioral performance

Accuracy and response times were very similar across all conditions. The 27 subjects included in the final analysis achieved >80% accuracy on each of the four conditions. To compute accuracy measures, trials in which the subject did not respond were considered incorrect. "No Response" trials were omitted from calculations involving response times. Across all subjects "No Response" trials only occurred 49 times out of 10,368 trials ($M \pm SD$ 1.73 ± 2.76 trials/subject). There was a statistically significant difference in accuracy between conditions as determined by a one-way ANOVA ($F(3, 26) = 4.241$, $P < 0.01$). Pairwise-T post hoc testing showed that accuracy on the perceptual matching condition was significantly lower than accuracy on the symbolic matching condition ($T(26) = -4.28$, $P < 0.01$) and the symbolic reasoning condition ($T(26) = -2.32$, $P < 0.05$). All other contrasts were found to not be significantly different from each other. Additionally, mean accuracy for each condition was above 92%, and considered to be at ceiling (symbolic reasoning: 94.7 ± 3.55% correct, symbolic matching: 96.0 ± 3.28% correct, perceptual reasoning: 94.7 ± 3.55% correct, perceptual matching: 92.8 ± 3.98% correct).

There was no significant difference in response times between conditions as determined by a one-way ANOVA, ($F(3, 26) = 2.02$, $P = 0.116$). Subjects' response times were consistent across the perceptual matching (1.74 ± 0.219 s), perceptual reasoning (1.79 ± 0.173 s), symbolic matching (1.67 ± 0.180 s), and symbolic reasoning (1.78 ± 0.231 s) conditions. Accuracy and response time measures are displayed in Supplementary Fig. S2. Overall, the behavioral results demonstrated that across all task conditions, subjects achieved high accuracy and similar response times, in line with our goal of generating different reasoning conditions with similar levels of difficulty.

Task-based fMRI

From previous research on abstract reasoning**,** we expected that frontoparietal cortex would be active during the reasoning conditions of our task. To test this, we generated brain activity maps using a univariate approach. Our results identified prefrontal regions and inferior temporal regions uniquely activated for symbolic and perceptual reasoning, respectively. The full results of the univariate analysis are described below.

Symbolic reasoning and symbol matching

A random-effects group analysis of the fMRI data contrasting the symbolic reasoning with the symbolic matching task conditions demonstrated significant clusters of increased signal (symbolic reasoning > symbolic matching) throughout left lateral prefrontal cortex (peak MNI coordinates = [−28, −2, 64] $Z = 6.60$), right lateral prefrontal cortex (peak MNI coordinates = [56, 10, 24], $Z = 5.37$), bilateral lateral parietal cortex/cerebellum (peak MNI coordinates = [48, −40, 54], $Z = 6.47$), bilateral dorsomedial prefrontal cortex (peak MNI coordinates = [−4, 26, 46], $Z = 5.48$), left anterior insula (peak MNI coordinates = [−38, 18, 0], $Z = 4.87$), and right frontal pole (peak MNI coordinates = [46, 52, −10], $Z = 4.47$). Significant negative clusters (symbolic matching > symbolic reasoning) were present in left medial prefrontal cortex (peak MNI coordinates = [−8, 54, −4], $Z = -5.17$), right medial prefrontal cortex (peak MNI coordinates = [−2, −46, 26], $Z = -4.71$), left frontopolar cortex (peak MNI coordinates [−24, 44, 42], $Z = -4.27$), and bilaterally in the precuneus (peak MNI coordinates = [2, −18, 42], $Z = -4.41$). Voxelwise activation maps are presented in Fig. 2A.

Perceptual reasoning and perceptual matching

A random-effects group analysis of the fMRI data contrasting the perceptual reasoning with the perceptual matching conditions of the task demonstrated significant positive clusters (perceptual reasoning > perceptual matching) throughout bilateral lateral parietal and inferior temporal cortices (peak MNI coordinates = [30, −60, −12], $Z = 6.41$), left dorsolateral prefrontal cortex (peak MNI coordinates = [−50, 36, 18], $Z = 4.37$), right dorsolateral prefrontal cortex (peak MNI coordinates = [−26, 6, 60], $Z = 4.77$), left cerebellum (peak MNI coordinates = [−28, −68, −52], $Z = 4.16$), and right cerebellum (peak MNI coordinates = [8, −56, −50] $Z = 4.60$). Significant negative clusters (perceptual matching > perceptual

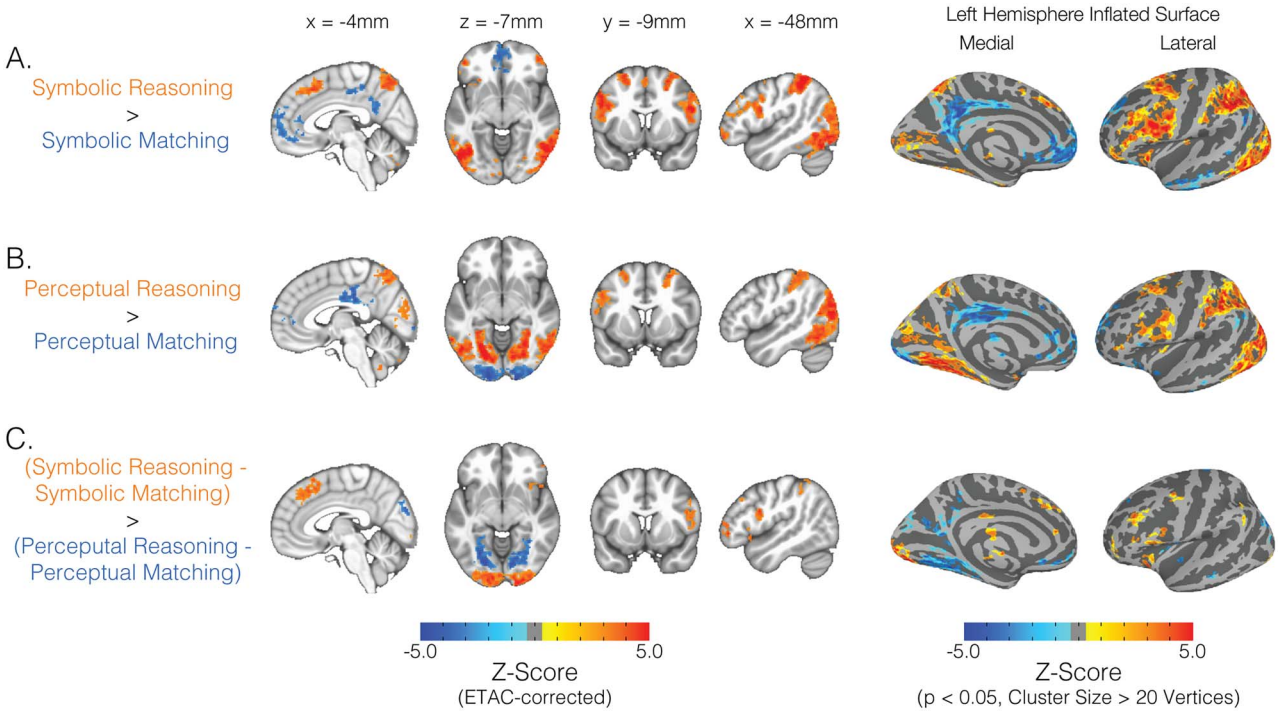

Fig. 2. fMRI activity maps. Shaded voxels indicate regions with a significant difference in activity between conditions for each of the following contrasts: A) The Symbolic Reasoning > Symbolic Matching contrast showed strong activation of frontoparietal cortex, and anterior prefrontal cortex. B) The Perceptual Reasoning > Perceptual Matching contrast showed strong activation of frontoparietal cortex and inferior temporal cortex. C) Interaction Maps (symbolic reasoning—matching) > (perceptual reasoning—perceptual matching) demonstrated that anterior prefrontal cortex was activated more strongly for symbolic processing, and inferior temporal cortex was activated more strongly for perceptual reasoning. Voxel shading represents Z-score magnitude. For the volumetric maps (left), activation was thresholded at $P < 0.05$ and corrected for multiple comparisons using AFNI's equitable thresholding and clustering (ETAC) method. Surface maps (right), shown for visualization purposes, were thresholded at $P < 0.05$, and for clusters with >20 vertices.

reasoning) were found in bilateral occipital cortex (peak MNI coordinates = [−18, −100, −8], $Z = -5.68$), left medial prefrontal cortex (peak MNI coordinates = [−4, 56, 16], $Z = -4.56$), and bilateral precuneus (peak MNI coordinates [2, −24, 36], $Z = -5.65$). Voxelwise activity maps are displayed in Fig. 2B.

Interaction maps

A random-effects group analysis of the fMRI data contrasting the symbolic conditions (symbolic reasoning > symbolic matching) with the perceptual conditions (perceptual reasoning > perceptual matching) was used to identify brain regions important for symbolic reasoning or perceptual reasoning as separate processes. Brain regions that were significant for symbolic reasoning included bilateral occipital cortex (peak MNI coordinates = [16, −100, 0], $Z = 5.72$), right dorsolateral prefrontal cortex and insula (peak MNI coordinates = [48, 8, 24], $Z = 4.58$), bilateral dorsomedial prefrontal cortex (peak MNI coordinates = [0, 34, 46], $Z = 5.20$), right lateral parietal cortex (peak MNI coordinates = [62, −32, 50], $Z = 4.14$), and right frontal pole (peak MNI coordinates = [48, 44, −2], $Z = 4.68$). Brain regions that were significantly more active for perceptual reasoning included bilateral parieto-occipital sulcus (peak MNI-coordinates = [12, −88, 28], $Z = -5.08$), right inferior temporal cortex (peak MNI-coordinates = [30, −58, −10], $Z = -5.74$), and left inferior temporal cortex (peak MNI-coordinates = [−20, −76, −8], $Z = -5.76$). Voxelwise activity maps are displayed in Fig. 2C.

Yeo-7 network ROI analysis

A region of interest (ROI) analysis was conducted to determine which functional brain networks (as defined by Yeo et al. 2011), were contributing to successful abstract reasoning behavior on the simplified Raven's Progressive Matrices task. ROI analysis showed increased activation in visual, dorsal attention, and cognitive control networks during the reasoning conditions compared to the matching conditions for both the symbolic and perceptual stimuli. Moreover, activation in the cognitive control network was greater for the symbolic contrast than for the perceptual contrast ($T = 3.48$, $P < 0.05$, Bonferroni corrected) (Fig. 3B). The results from this analysis are shown in Fig. 3.

Network reconfiguration

We performed a network reconfiguration analysis based on work by Hearne et al. (2017). An alluvial flow plot in Fig. 4 displays the results from this analysis. Using Louvain community detection, we identified 11 communities during resting state (A–K), and 3 communities during each of the 4 task conditions (A–C). During pre-task resting state, the communities roughly correspond to the default network (community A), somatomotor network (community B), visual network (community C), along with 8 communities (D–K) that when combined, form the frontoparietal networks dorsal attention, ventral attention, and cognitive control (Yeo et al. 2011). During the task, communities A and B remained largely intact, trading a small number of nodes with the frontoparietal communities (see Fig. 4). The remaining task community (community C) formed a robust frontoparietal-visual system from the strengthened connections among resting state communities C–K, reflecting stronger connections between frontoparietal and visual nodes during the task compared to rest. In Fig. 5A, we show the topography of each community A–C for the symbolic reasoning condition of the task. This topography is nearly identical to

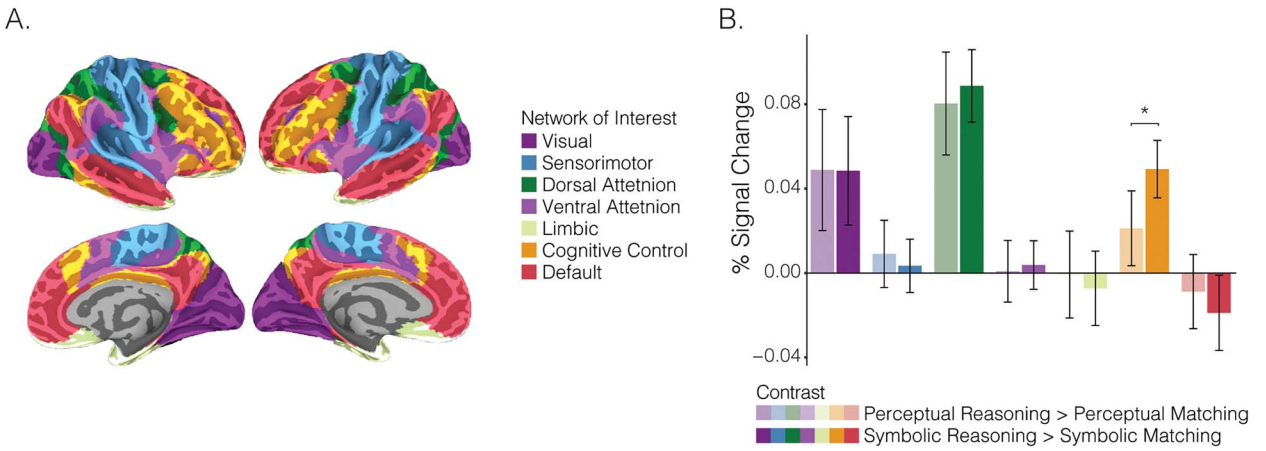

Fig. 3. Resting state network ROI analysis. A) Regions of interest were defined a priori from the Yeo 7-network resting state parcellation (2011). B) Bars represent BOLD percent signal change in each ROI for the perceptual contrast (lighter colors), and symbolic contrast (darker colors). Visual, dorsal attention, and cognitive control networks showed increased activation for both contrasts. Activation of the cognitive control network was higher for the symbolic contrast compared to the perceptual contrast. Error bars indicated 95% confidence interval. * denotes significant difference in percent signal change between contrasts ($P < 0.05$, Bonferroni corrected for multiple comparisons).

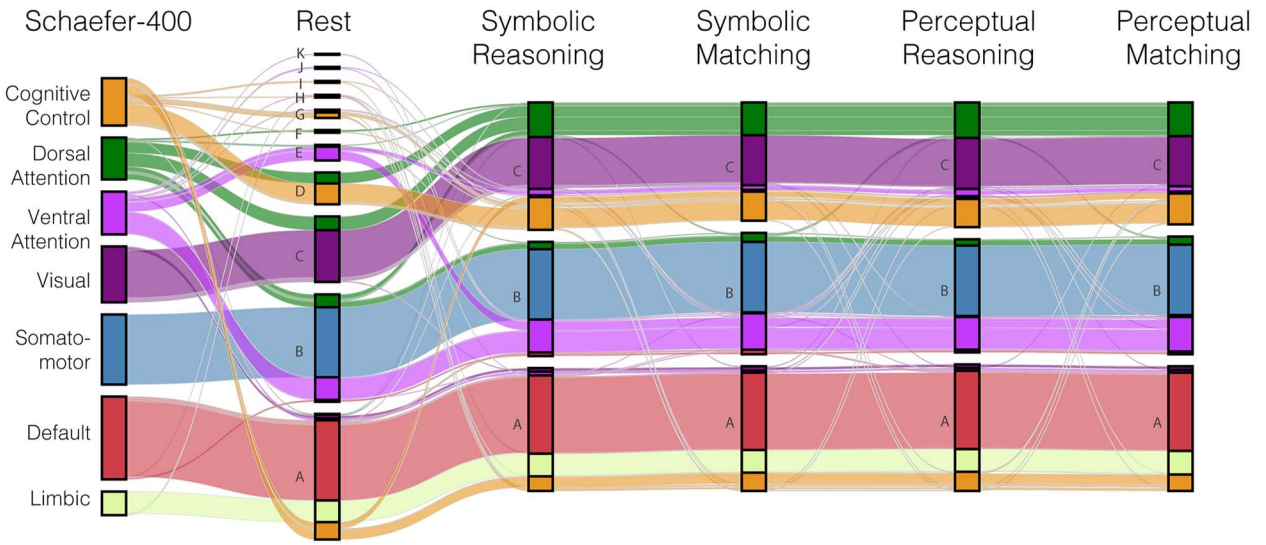

Fig. 4. Task-based network reconfiguration. We plotted network reconfiguration on an alluvial flow diagram to demonstrate the changing community memberships of nodes in the brain network. Canonical community memberships are shown in the left column for the 400 ROIs in the Schaefer-400 cortical parcellation with Yeo-7 labels (Schaefer et al. 2018). A Louvain community detection algorithm was used to define network communities during resting state and each of the four task conditions (labeled here as respective columns in the flow diagram). During resting state, the brain network was divided into 11 communities (labeled A—K). During each task condition, three communities (A—C) were detected. Notably, cognitive control nodes showed a fragmented community structure during resting state, and joined together with dorsal attention and visual nodes to form a stable task community during all four task conditions. Connecting flows show the changing community memberships across rest and task conditions. To visualize the makeup of each community, colors represent the canonical Yeo-7 memberships for each of the Schaefer-400 regions (Orange = Cognitive Control, Green = Dorsal Attention, Violet = Ventral Attention, Purple = Visual, Blue = Somatomotor, Red = Default, Cream = Limbic).

communities A–C in each of the other three task conditions (not shown).

Follow-up analyses demonstrated that scanning parameters had little to no effect on the fractionated frontoparietal community structure observed during resting state. Like the original analysis, we observed stable communities that roughly correspond to the default network (community A) and the somatomotor network (community B), along with multiple smaller communities that when combined, form the frontoparietal networks. These results were consistent when analyzing each resting state run separately and when downsampling the resting state data (see Supplementary Fig. S3).

Using the variation of information metric (V_{In}), we quantified the similarity between the community partitions for each of the task conditions and the resting state. When considering the entire brain network, we found that the community structure during each of the 4 task conditions was significantly different from the community structure during resting state (V_{In} symbolic reasoning vs. rest = 0.17; V_{In} symbolic matching vs. rest = 0.17; V_{In} perceptual reasoning vs. rest = 0.18; V_{In} perceptual matching vs. rest = 0.17; $P < 0.01$, Bonferroni corrected for all contrasts).

Since the whole-brain community structure was significantly different between rest and the task conditions, we quantified the relative amount of reconfiguration in task communities A–C. To do so, we calculated V_{In} individually for each task community across each of the 4 task conditions (see Fig. 5B). All *P*-values were Bonferroni-corrected for multiple comparisons. A repeated measures ANOVA showed a main effect of task

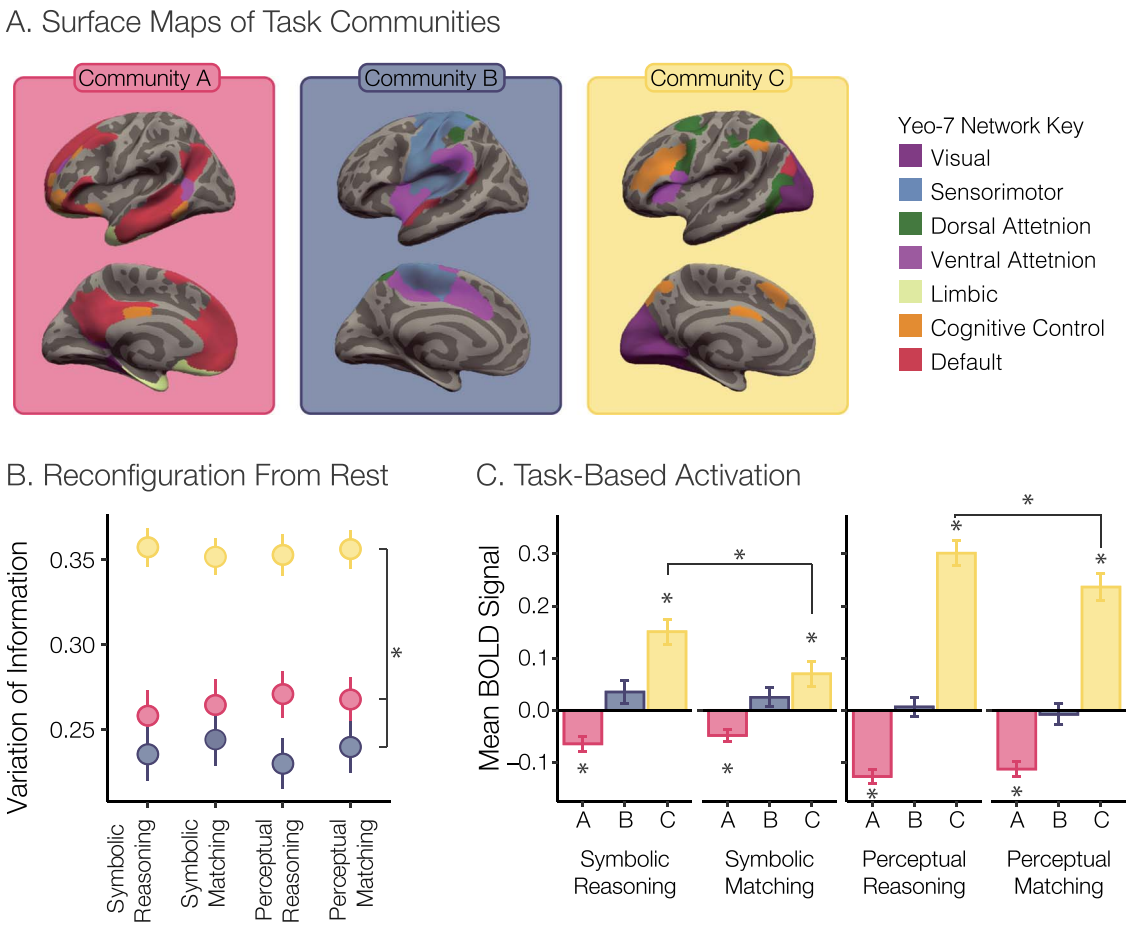

Fig. 5. Community layout, reconfiguration, and activity. A) Three communities were detected during each of the task conditions. Projected here on a cortical surface are the communities from the symbolic reasoning condition. Individual nodes from the Schaefer-400 cortical parcellation are colored according to their canonical Yeo-7 network membership (Schaefer et al. 2018). Although only the communities for symbolic reasoning are shown here, the condition-specific A, B, and C communities were used to calculate the statistics shown in panels B and C. B) To quantify the amount of community reconfiguration between each task condition and the resting state we plotted the variation of information (V_{In}) for each of the task communities. Points represent mean V_{In} across subjects. Error bars represent standard error. Nodes in community C showed the largest change in community assignment for all four conditions, compared to rest. * denotes significant differences in V_{In} between communities ($P < 0.05$, Bonferroni corrected). C) The mean BOLD signal (compared to the inter-trial interval) within each task community is plotted for each of the task conditions. Community C was the only community that showed significant differences in activation between Reasoning and Matching conditions. Bar height represents the mean BOLD signal across subjects for each community. Error bars represent standard error. Across all graphs, Red = community A, Blue = community B, Yellow = community C. * denotes mean BOLD signal significantly different from zero ($P < 0.05$, Bonferroni corrected). Notably, community C showed both the largest amount of reconfiguration (panel B) and the highest task-based activation (panel C).

community ($F(2,26) = 30.78$, $P < 0.01$) but no main effect of task condition ($F(3,26) = 0.717$, $P = 1.0$). Post-hoc testing with pairwise t-tests showed that across all four task conditions, community C (the frontoparietal-visual community) had the highest overall V_{In} and that it was significantly higher than the V_{In} of both other task communities (compared to community A: $T(134) = 14.99$, $P < 0.01$, and compared to community B: $T(134) = 16.19$, $P < 0.01$). Additionally, there was also a significant difference in the V_{In} metric between communities A and B ($T(134) = 2.86$), ($P < 0.05$). Together, these results demonstrate that the change in community structure between resting state and the reasoning task is driven by reconfiguration of nodes in community C (the frontoparietal-visual community) (see Fig. 5B).

ROI analysis of reconfigured communities

To determine how each of the communities differentially contributed to the various reasoning conditions, we calculated the average BOLD signal within each community for each of the four task conditions (see Fig. 5C). All P-values below are Bonferroni-corrected for multiple comparisons.

A repeated measures ANOVA showed significant differences in the activity of community A across the four task conditions ($F(3,26) = 29.15$, $P < 0.01$). Post-hoc analysis demonstrated significant differences between symbolic reasoning vs. perceptual reasoning ($T(26) = 6.65$, $P < 0.01$), symbolic reasoning vs. perceptual matching ($T(26) = 5.18$, $P < 0.01$), symbolic matching vs. perceptual reasoning ($T(26) = 6.60$, $P < 0.01$), and symbolic matching vs. perceptual matching ($T(26) = 6.98$, $P < 0.01$).

A repeated measures ANOVA also showed significant differences in the activity of community B across the 4 task conditions ($F(3,26) = 9.33$, $P < 0.01$). Post-hoc analysis showed significant differences between symbolic reasoning vs. perceptual matching ($T(26) = 5.31$, $P < 0.01$), and symbolic matching vs. perceptual matching ($T(26) = 3.87$, $P < 0.01$).

Finally, a repeated measures ANOVA showed significant differences in the activity of community C across the four task conditions ($F(3,26) = 92.24$, $P < 0.01$). Notably, community C showed the highest levels of activity on the task, and post-hoc analysis showed that it was the only community with significant activity differences for symbolic reasoning > symbolic

matching and perceptual reasoning > perceptual matching. Post-hoc analysis demonstrated significant differences between all six contrasts: symbolic reasoning vs. symbolic matching ($T(26) = 9.05$, $P < 0.01$), symbolic reasoning vs. perceptual reasoning ($T(26) = -11.20$, $P < 0.01$), symbolic reasoning vs. perceptual matching ($T(26) = -4.74$, $P < 0.01$), symbolic matching vs. perceptual reasoning ($T(26) = -16.50$, $P < 0.01$), symbolic matching vs. perceptual matching ($T(26) = -9.12$, $P < 0.01$), and perceptual reasoning vs. perceptual matching ($T(26) = 4.52$, $P < 0.01$).

Together, these results demonstrate that each community identified in the network reconfiguration analysis has an activity pattern that is consistent in its direction, always positively activated or negatively activated, but variable in its intensity across the task conditions. Namely, community A (default) is negatively activated, community B (somatomotor) is not significantly activated, and community C (frontoparietal-visual) is positively activated. Community C showed increased activity during symbolic and perceptual reasoning conditions compared to their respective matching conditions (see Fig. 5C).

Discussion

In this study, we investigated regional variability in brain network activation and functional network reconfiguration between resting-state and abstract reasoning. By analyzing fMRI data during both resting and task states, we demonstrated that default and somatomotor networks remained stable, while frontoparietal and visual networks flexibly reconfigured into a task-ready state. When examining task-based activity patterns, we found that frontoparietal and visual networks, which had flexibly reconfigured from resting to task states, exhibited the strongest task-based activation. These results demonstrated that flexible reconfiguration of underlying networks supports the transition from rest to task, and that activation of frontoparietal cortex supports abstract reasoning.

A stable network core persists during rest and the task

Consistent with prior work, we found that overall, functional brain network topology was largely conserved between resting state and task (Cole et al. 2014; Krienen et al. 2014; Hearne et al. 2017; Gratton, Laumann, et al. 2018a; Salvo et al. 2021). Across both resting state and task scans, we identified 2 stable communities primarily consisting of regions in the default and somatomotor networks (see Fig. 4). Previous work suggests that these regions form a stable network "core" and that they exhibit the fewest changes in functional connectivity when comparing resting and task states (Krienen et al. 2014). Recent work from our lab further suggests that successful rule learning ability is associated with increased stability of specific brain networks, including the somatomotor network (Morin et al. 2021). Previous work has shown that increased whole-brain network stability between resting and task states is strongly associated with higher fluid intelligence scores (Schultz and Cole 2016; Ferguson et al. 2017; Hilger et al. 2020; Thiele et al. 2021). As a working hypothesis, we propose that stability in somatomotor and default regions allows the brain to spend more energy reconfiguring the functional connectivity of other regions, such as frontoparietal and visual cortices, that show increased activation during the task. Future studies employing network control theory (Gu et al. 2015; Scheid et al. 2021) or activity flow mapping (Cole et al. 2016) may be able to model the "energy savings" that are afforded when the underlying functional connectivity network is reconfigured into a task-ready state.

Frontoparietal and visual cortices flexibly reconfigure to support reasoning

During the resting state scans, we found a largely fragmented community structure among frontoparietal and visual regions, consisting of 9 small communities. While these regions were part of many different communities at rest, they joined together to form a single strongly connected community during the task (see Fig. 4). This task-based community was maintained across all four task conditions. This result is consistent with previous work from Hearne and colleagues, who found that frontoparietal and visual cortical regions exhibited increased reconfiguration, forming a single community structure during a Latin Squares reasoning task (2017). Previous work has shown that generally, frontoparietal cortex shows increased reconfiguration compared to other brain regions, and that increased flexibility of frontoparietal cortex is associated with better performance on motor sequence learning, associative learning, and working memory tasks (Bassett et al. 2011; Braun et al. 2015; Betzel et al. 2017; Gerraty et al. 2018). Moreover, patterns of task-based network reconfiguration occurring in frontoparietal control regions is predictive of individual differences in fluid intelligence scores (Greene et al. 2018).

Frontoparietal cortical regions are uniquely positioned to integrate information across distal regions of cortex (for review, see Parks and Madden 2013; Avena-Koenigsberger et al. 2017). During abstract reasoning, the brain must balance global integration of information with local specialization. Functional brain networks facilitate this balance with a rich-club organization where hub regions, regions with strong network-wide connectivity, are also highly interconnected with each other (van den Heuvel and Sporns 2011). Frontoparietal cortex contains hubs that are well-positioned to facilitate interaction between functional networks (Gratton, Sun, et al. 2018b). Previous work has demonstrated that the brain adaptively shifts between various task demands by flexibly altering global functional connectivity patterns functional with hubs in the frontoparietal control network (Cole et al. 2013). We propose that the formation of a strong frontoparietal-visual community facilitates the brain-wide integration of visuospatial information across networks.

Frontoparietal network activity and reconfiguration supports reasoning

In our study, frontoparietal cortex was significantly more active for reasoning conditions compared to matching conditions (see Fig. 5). Moreover, activation of the cognitive control network, as defined a priori in the Yeo-7 atlas, was greater for the symbolic reasoning contrast compared to the perceptual reasoning contrast (see Fig. 3). Frontoparietal cortical regions are known to be activated in a variety of abstract reasoning paradigms including tasks of analogical reasoning (Green et al. 2010; Watson and Chatterjee 2012), rule learning (Wallis et al. 2001), and matrix reasoning (Prabhakaran et al. 1997; Christoff et al. 2001; Melrose et al. 2007, 2018; Golde et al. 2010). Functional MRI studies have demonstrated lateral parietal activity during tasks of top-down directed attention (Bisley and Goldberg 2003), mental rotation and spatial reasoning (Schendan and Stern 2007, 2008), and magnitude processing (including numerical, temporal, and spatial magnitudes) (Walsh 2003; Ansari et al. 2006; Holloway et al. 2010; Maloney et al. 2010; Van Opstal and Verguts 2013; Sokolowski et al. 2017). Lateral prefrontal cortex has also been implicated in abstract

reasoning behavior and previous studies have demonstrated activation associated with increased rule complexity, relational integration, and working memory demands (Prabhakaran et al. 1997; Christoff et al. 2001; Bunge et al. 2009; Wendelken et al. 2012). More generally, researchers have proposed that frontoparietal cortex functionally contributes to general human intelligence, which is often measured with abstract reasoning tasks similar to the one used in our experiment (Jung and Haier 2007; Vakhtin et al. 2014; Fraenz et al. 2021).

In addition to robust evidence linking frontoparietal activation to reasoning, previous work has shown that activation in lateral and medial prefrontal cortex is linked to time-on-task (Christoff et al. 2001; Grinbrand et al. 2011; Gilbert et al. 2012). The reasoning task used in our study was specifically designed to match response times across conditions, so that brain activation patterns were related to reasoning, rather than time-on-task. Building off previous work, we show that even when response-times were controlled for, reasoning reliably activated frontoparietal cortex. Additionally, symbolic reasoning activated frontoparietal cortex more strongly than perceptual reasoning.

Highly activated regions exhibited the greatest network reconfiguration

We found that the cognitive control network not only increased activation during symbolic and perceptual reasoning, but also increased reconfiguration between resting and task states (see Fig. 5). These frontoparietal cognitive control nodes enjoy a privileged hub status within functional brain networks, with increased functional connectivity to each other and to many regions throughout the brain (van den Heuvel and Sporns 2011). Previous work proposed that network nodes exhibiting both hub status and increased task activation are uniquely positioned to exert cognitive control (Gratton et al. 2016). Because of their widely distributed connections to many other brain networks, hub nodes have the ability to influence large-scale activation patterns. We propose that the robust community structure of frontoparietal hub nodes that formed during the task facilitates the integration of information across distal brain regions and results in increased task activation of the community.

Notably, the regions that showed the largest task-based community reconfiguration also showed the largest magnitude change in task-based activation (see Fig. 5), suggesting that task-related co-activation could increase coupling between brain regions. Through our denoising and weighted-GLM procedures for calculating task-based functional connectivity (see section Methods for details), we attempted to ensure that functional connectivity measures were separate from task-based co-activation. At a theoretical level, we propose that the reconfiguration of these functional networks when transitioning from rest to task occurs in order to facilitate more efficient task activation. Previous studies using connectome fingerprinting have established that resting-state functional connectivity is predictive of task-based activation (Tobyne et al. 2018; Osher et al. 2019; Porter et al. 2022). Moreover, individual network connectivity is predictive of task-based activity patterns (Salvo et al. 2021). Modeling work using activity flow mapping has also shown that task activation patterns can be predicted from the underlying network of functional connectivity (Cole et al. 2016). Studies have also shown that changes to the underlying functional connectome (e.g. due to task-reconfiguration) can affect task activation patterns (Arbabshirani et al. 2013; Tomasi and Volkow 2019; Cole et al. 2021). Together with this previous literature, our results suggest that task activations occur along with an underlying functional connectivity network that has been flexibly reconfigured into a task-ready state.

Citation diversity statement

Recent work in neuroscience has identified a bias in citation practices such that papers from women and other minority scholars are under-cited relative to the number of such papers in the field (Dworkin, Linn, et al. 2020a; Dworkin, Zurn, et al. 2020b). Here we quantify the citation diversity of the present manuscript excluding self-citations of the first and last authors of this manuscript. Our reference list contains 9.49% woman-woman (first author-last author), 11.8% man-woman, 20.0% woman–man, and 58.7% man–man. This method is limited in that (i) names, pronouns, and social media profiles used to construct the databases may not, in every case, be indicative of gender identity and (ii) it cannot account for intersex, non-binary, or transgender people. Our reference list contains 6.58% author of color (first)/author of color(last), 15.3% white author/author of color, 21.0% author of color/white author, and 57.13% white author/white author. This method is limited in that (i) names and Florida Voter Data to make the predictions may not be indicative of racial/ethnic identity, and (ii) it cannot account for Indigenous and mixed-race authors, or those who may face differential biases due to the ambiguous racialization or ethnicization of their names. Methodological details of how we obtained these estimates can be found in Zhou et al. (2020). We look forward to future work that supports equitable practices in science.

Supplementary material

Supplementary material is available at *Cerebral Cortex* online.

Acknowledgements

The authors would like to thank Matthew F. Dunne, Stamatios S.P. Liapis, Caroline Ahn, Dr Allen E. Chang, Dr Rachel K. Nauer, Dr Joseph T. McGuire, Dr David Badre, Dr David C. Somers, and Dr Michael E. Hasselmo for their comments and feedback during the preparation of this manuscript. Additionally, the authors would like to thank Shruthi Chakrapani and Dr Jason W. Bohland for their assistance in data collection and MRI scanning.

Funding

This work was supported by the Office of Naval Research (grant numbers MURI N00014-16-1-2832, DURIP N00014-17-2304), and the National Science Foundation (grant number 1625552).

Conflict of interest statement: The authors declare no competing financial interests.

References

Ansari D, Fugelsang JA, Dhital B, Venkatraman V. Dissociating response conflict from numerical magnitude processing in the brain: an event-related fMRI study. *NeuroImage*. 2006:32(2):799–805. https://doi.org/10.1016/J.NEUROIMAGE.2006.04.184.

Arbabshirani MR, Havlicek M, Kiehl KA, Pearlson GD, Calhoun VD. Functional network connectivity during rest and task conditions: A comparative study. *Hum Brain Mapp*. 2013:34(11):2959–2971. https://doi.org/10.1002/HBM.22118.

Avena-Koenigsberger A, Misic B, Sporns O. Communication dynamics in complex brain networks. *Nat Rev Neurosci*. 2017:19(1):17–33. https://doi.org/10.1038/nrn.2017.149.

Badre D, D'Esposito M. Functional magnetic resonance imaging evidence for a hierarchical organization of the prefrontal cortex. *J Cogn Neurosci*. 2007:19(12):2082–2099. https://doi.org/10.1162/jocn.2007.19.12.2082.

Badre D, D'Esposito M. Is the rostro-caudal axis of the frontal lobe hierarchical? *Nat Rev Neurosci*. 2009:10(9):659–669. https://doi.org/10.1038/nrn2667.

Badre D, Nee DE. Frontal cortex and the hierarchical control of behavior. *Trends Cogn Sci*. 2018:22(2):170–188. https://doi.org/10.1016/j.tics.2017.11.005.

Bassett DS, Wymbs NF, Porter MA, Mucha PJ, Carlson JM, Grafton ST. Dynamic reconfiguration of human brain networks during learning. *Proc Natl Acad Sci*. 2011:108(18):7641–7646. https://doi.org/10.1073/pnas.1018985108.

Betzel RF, Satterthwaite TD, Gold JI, Bassett DS. Positive affect, surprise, and fatigue are correlates of network flexibility. *Sci Rep*. 2017:7(1):1–10. https://doi.org/10.1038/s41598-017-00425-z.

Bisley JW, Goldberg ME. Neuronal activity in the lateral intraparietal area and spatial attention. *Science*. 2003:299(5603):81–86. https://doi.org/10.1126/science.1077395.

Braun U, Schäfer A, Walter H, Erk S, Romanczuk-Seiferth N, Haddad L, Schweiger JI, Grimm O, Heinz A, Tost H, et al. Dynamic reconfiguration of frontal brain networks during executive cognition in humans. *Proc Natl Acad Sci*. 2015:112(37):11678–11683. https://doi.org/10.1073/pnas.1422487112.

Bunge SA, Helskog EH, Wendelken C. Left, but not right, rostrolateral prefrontal cortex meets a stringent test of the relational integration hypothesis. *NeuroImage*. 2009:46(1):338–342. https://doi.org/10.1093/cercor/bhh126.

Bunge SA, Wendelken C, Badre D, Wagner AD. Analogical reasoning and prefrontal cortex: evidence for separable retrieval and integration mechanisms. *Cereb Cortex*. 2005:15(3):239–249. https://doi.org/10.1016/J.NEUROIMAGE.2009.01.064.

Cauley S, Polimeni J, Bhat H, Wald L, Setsompop K. Interslice leakage artifact reduction technique for simultaneous multislice acquisitions. *Magn Reson Med*. 2014:72(1):93–102.

Chai XJ, Castañón AN, Öngür D, Whitfield-Gabrieli S. Anticorrelations in resting state networks without global signal regression. *NeuroImage*. 2012:59(2):1420. https://doi.org/10.1016/J.NEUROIMAGE.2011.08.048.

Christoff K, Prabhakaran V, Dorfman J, Zhao Z, Kroger JK, Holyoak KJ, Gabrieli JDE. Rostrolateral prefrontal cortex involvement in relational integration during reasoning. *NeuroImage*. 2001:14(5):1136–1149. https://doi.org/10.1006/nimg.2001.0922.

Ciric R, Thompson WH, Lorenz R, Goncalves M, MacNicol E, Markiewicz CJ, Halchenko YO, Ghosh SS, Gorgolewski KJ, Poldrack RA, et al. TemplateFlow: FAIR-sharing of multi-scale, multi-species brain models. *BioRxiv*. 2021:1–27. https://doi.org/10.1101/2021.02.10.430678.

Cohen JE, Ross RS, Stern CE. Predictability matters: role of the hippocampus and prefrontal cortex in disambiguation of overlapping sequences. *Learn Mem*. 2018:25(8):335–346. https://doi.org/10.1101/LM.047175.117.

Cole MW, Bassett DS, Power JD, Braver TS, Petersen SE. Intrinsic and task-evoked network architectures of the human brain. *Neuron*. 2014:83(1):238–251. https://doi.org/10.1016/J.NEURON.2014.05.014.

Cole MW, Ito T, Bassett DS, Schultz DH. Activity flow over resting-state networks shapes cognitive task activations. *Nat Neurosci*. 2016:19(12):1718. https://doi.org/10.1038/NN.4406.

Cole MW, Ito T, Cocuzza C, Sanchez-Romero R. The functional relevance of task-state functional connectivity. *J Neurosci*. 2021:41(12):2684–2702. https://doi.org/10.1523/JNEUROSCI.1713-20.2021.

Cole MW, Reynolds JR, Power JD, Repovs G, Anticevic A, Braver TS. Multi-task connectivity reveals flexible hubs for adaptive task control. *Nat Neurosci*. 2013:16:1348–1355. https://doi.org/10.1038/nn.3470.

Cox RW. Equitable thresholding and clustering: a novel method for functional magnetic resonance imaging clustering in AFNI. *Brain Connect*. 2019:9(7):529–538. https://doi.org/10.1089/brain.2019.0666.

Do Q, Hasselmo ME. Neural circuits and symbolic processing. *Neurobiol Learn Mem*. 2021:186:107552. https://doi.org/10.1016/J.NLM.2021.107552.

Dworkin JD, Linn KA, Teich EG, Zurn P, Shinohara RT, Bassett DS. The extent and drivers of gender imbalance in neuroscience reference lists. *Nat Neurosci*. 2020a:23(8):918–926. https://doi.org/10.1038/s41593-020-0658-y.

Dworkin JD, Zurn P, Bassett DS. (In)citing action to realize an equitable future. *Neuron*. 2020b:106:890–894. https://doi.org/10.1016/j.neuron.2020.05.011.

Esteban O, Markiewicz CJ, Blair RW, Moodie CA, Isik AI, Erramuzpe A, Kent JD, Goncalves M, DuPre E, Snyder M, et al. fMRIPrep: a robust preprocessing pipeline for functional MRI. *Nat Methods*. 2019:16(1):111–116. https://doi.org/10.1038/s41592-018-0235-4.

Feinberg DA, Moeller S, Smith SM, Auerbach EJ, Ramanna S, Glasser MF, Miller KL, Ugurbil K, Yacoub E. Multiplexed echo planar imaging for sub-second whole brain FMRI and fast diffusion imaging. *PLoS One*. 2010:5:e15710.

Ferguson MA, Anderson JS, Spreng RN. Fluid and flexible minds: intelligence reflects synchrony in the brain's intrinsic network architecture. *Network Neurosci*. 2017:1(2):192–207. https://doi.org/10.1162/netn_a_00010.

Fischl B. FreeSurfer. *NeuroImage*. 2012:62(2):774–781. https://doi.org/10.1016/j.neuroimage.2012.01.021.

Fortunato S. Community detection in graphs. *Phys Rep*. 2010:486(3–5):75–174. https://doi.org/10.1016/J.PHYSREP.2009.11.002.

Fraenz C, Schlüter C, Friedrich P, Jung RE, Güntürkün O, Genç E. Interindividual differences in matrix reasoning are linked to functional connectivity between brain regions nominated by Parieto-Frontal Integration Theory. *Intelligence*. 2021:87:101545. https://doi.org/10.1016/J.INTELL.2021.101545.

Garrison KA, Scheinost D, Finn ES, Shen X, Constable RT. The (in)stability of functional brain network measures across thresholds. *NeuroImage*. 2015:118:651–661. https://doi.org/10.1016/J.NEUROIMAGE.2015.05.046.

Gerraty RT, Davidow JY, Foerde K, Galvan A, Bassett DS, Shohamy D. Dynamic flexibility in striatal-cortical circuits supports reinforcement learning. *J Neurosci*. 2018:38(10):2442–2453. https://doi.org/10.1523/JNEUROSCI.2084-17.2018.

Gilbert SJ, Bird G, Frith CD, Burgess PW. Does "task difficulty" explain "task-induced deactivation?". *Front Psychol*. 2012:3:1–12. https://doi.org/10.3389/fpsyg.2012.00125.

Golde, M., von Cramon, D. Y., & Schubotz, R. I. (2010). Differential role of anterior prefrontal and premotor cortex in the processing of relational information. *NeuroImage*, 49, 2890–2900. https://ac.els-cdn.com/S1053811909009884/1-s2.0-S1053811909009884-main.pdf?_tid=97aed7e8-d9ef-11e7-a3e2-00000aacb361&acdnat=1512501052_d09f4fc9870e53ff7fcf531f3e7547f0.

Gonzalez-Castillo J, Bandettini PA. Task-based dynamic functional connectivity: recent findings and open questions. *NeuroImage*. 2018:180:526–533. https://doi.org/10.1016/J.NEUROIMAGE.2017.08.006.

Gratton C, Laumann TO, Gordon EM, Adeyemo B, Petersen SE. Evidence for two independent factors that modify brain networks to meet task goals. *Cell Rep*. 2016:17(5):1276–1288. https://doi.org/10.1016/j.celrep.2016.10.002.

Gratton C, Laumann TO, Nielsen AN, Greene DJ, Gordon EM, Gilmore AW, Nelson SM, Coalson RS, Snyder AZ, Schlaggar BL, et al. Functional brain networks are dominated by stable group and individual factors, not cognitive or daily variation. *Neuron*. 2018a:98(2):439–452.e5. https://doi.org/10.1016/J.NEURON.2018.03.035.

Gratton C, Sun H, Petersen SE. Control networks and hubs. *Psychophysiology*. 2018b:55(3):1–18. https://doi.org/10.1111/psyp.13032.

Green AE, Kraemer DJM, Fugelsang JA, Gray JR, Dunbar KN. Connecting long distance: semantic distance in analogical reasoning modulates frontopolar cortex activity. *Cereb Cortex*. 2010:20(1):70–76. https://doi.org/10.1093/cercor/bhp081.

Greene AS, Gao S, Scheinost D, Constable RT. Task-induced brain state manipulation improves prediction of individual traits. *Nature Commun*. 2018:9(1):1–13. https://doi.org/10.1038/s41467-018-04920-3.

Grinbrand J, Savitskaya J, Wager TD, Teichert T, Ferrera VP, Hirsch J. The dorsal medial frontal cortex is sensitive to time on task, not response conflict or error likelihood. *NeuroImage*. 2011:57(2):303–311. https://doi.org/10.1016/j.neuroimage.2020.12.027.

Gu S, Pasqualetti F, Cieslak M, Telesford QK, Yu AB, Kahn AE, Medaglia JD, Vettel JM, Miller MB, Grafton ST, et al. Controllability of structural brain networks. *Nat Commun*. 2015:6(1):1–10. https://doi.org/10.1038/ncomms9414.

Hasselmo ME, Stern CE. A network model of behavioural performance in a rule learning task. *Philos Trans R Soc B Biol Sci*. 2018:373(1744):1–10. https://doi.org/10.1098/RSTB.2017.0275.

Hearne LJ, Cocchi L, Zalesky A, Mattingley JB. Interactions between default mode and control networks as a function of increasing cognitive reasoning complexity. *Hum Brain Mapp*. 2015:36(7):2719–2731. https://doi.org/10.1002/hbm.22802.

Hearne LJ, Cocchi L, Zalesky A, Mattingley JB. Reconfiguration of brain network architectures between resting-state and complexity-dependent cognitive reasoning. *J Neurosci*. 2017:37(35):8399–8411. https://doi.org/10.1523/JNEUROSCI.0485-17.2017.

Hilger K, Fukushima M, Sporns O, Fiebach CJ. Temporal stability of functional brain modules associated with human intelligence. *Hum Brain Mapp*. 2020:41(2):362–372. https://doi.org/10.1002/HBM.24807.

Holloway ID, Price GR, Ansari D. Common and segregated neural pathways for the processing of symbolic and nonsymbolic numerical magnitude: an fMRI study. *NeuroImage*. 2010:49(1):1006–1017. https://doi.org/10.1016/J.NEUROIMAGE.2009.07.071.

Hoshi E, Shima K, Tanji J. Neuronal activity in the primate prefrontal cortex in the process of motor selection based on two behavioral rules. *J Neurophysiol*. 2000:83(4):2355–2373. https://doi.org/10.1152/jn.2000.83.4.2355.

Jung RE, Haier RJ. The Parieto-Frontal Integration Theory (P-FIT) of intelligence: converging neuroimaging evidence. *Behav Brain Sci*. 2007:30(2):135–154. https://doi.org/10.1017/S0140525X07001185.

Krienen FM, Thomas Yeo BT, Buckner RL. Reconfigurable task-dependent functional coupling modes cluster around a core functional architecture. *Philos Trans R Soc B Biol Sci*. 2014:369(1653):1–14. https://doi.org/10.1098/RSTB.2013.0526.

Kroger J, Sabb F, Fales C, Bookheimer S, Cohen M, Holyoak K. Recruitment of anterior dorsolateral prefrontal cortex in human reasoning: a parametric study of relational complexity. *Cereb Cortex*. 2002:12(5):477–485.

Maloney EA, Risko EF, Preston F, Ansari D, Fugelsang J. Challenging the reliability and validity of cognitive measures: the case of the numerical distance effect. *Acta Psychol*. 2010:134(2):154–161. https://doi.org/10.1016/J.ACTPSY.2010.01.006.

Mansouri FA, Freedman DJ, Buckley MJ. Emergence of abstract rules in the primate brain. *Nat Rev Neurosci*. 2020:21(11):595–610. https://doi.org/10.1038/s41583-020-0364-5.

Meilă M. Comparing clusterings—an information based distance. *J Multivar Anal*. 2007:98(5):873–895. https://doi.org/10.1016/J.JMVA.2006.11.013.

Melrose RJ, Jimenez AM, Riskin-Jones H, Weissberger G, Veliz J, Hasratian AS, Wilkins S, Sultzer DL. Alterations to task positive and task negative networks during executive functioning in mild cognitive impairment. *NeuroImage Clin*. 2018:19:970. https://doi.org/10.1016/J.NICL.2018.06.014.

Melrose RJ, Poulin RM, Stern CE. An fMRI investigation of the role of the basal ganglia in reasoning. *Brain Res*. 2007:1142:146–158. https://doi.org/10.1016/j.brainres.2007.01.060.

Moeller S, Yacoub E, Olman CA, Auerbach E, Strupp J, Harel N, Uğurbil K. Multiband multislice GE-EPI at 7 Tesla with 16-fold acceleration using Partial Parallel Imaging with application to high spatial and temporal whole-brain FMRI. *Magn Reson Med*. 2010:63:1144–1153.

Morin TM, Chang AE, Ma W, McGuire JT, Stern CE. Dynamic network analysis demonstrates the formation of stable functional networks during rule learning. *Cereb Cortex*. 2021:31(12):5511–5525. https://doi.org/10.1093/CERCOR/BHAB175.

Newman MEJ, Girvan M. Finding and evaluating community structure in networks. *Phys Rev E*. 2004:69(026113):1–15. https://doi.org/10.1103/PhysRevE.69.026113.

Osher DE, Brissenden JA, Somers DC. Predicting an individual's dorsal attention network activity from functional connectivity fingerprints. *J Neurophysiol*. 2019:122(1):232–240. https://doi.org/10.1152/JN.00174.2019.

Parks EL, Madden DJ. Brain connectivity and visual attention. *Brain Connect*. 2013:3(4):317–338. https://doi.org/10.1089/BRAIN.2012.0139.

Peirce JW. PsychoPy—psychophysics software in Python. *J Neurosci Methods*. 2007:162(1–2):8–13. https://doi.org/10.1016/j.jneumeth.2006.11.017.

Peirce JW. Generating stimuli for neuroscience using PsychoPy. *Front Neuroinform*. 2009:2:1–8. https://doi.org/10.3389/neuro.11.010.2008.

Porter A, Nielsen A, Dorn M, Dworetsky A, Edmonds D, Gratton C. Masked features of task states found in individual brain networks. *Cerebral Cortex*. 2022. https://doi.org/10.1093/cercor/bhac247.

Prabhakaran V, Smith JAL, Desmond JE, Glover GH, Gabrieli JDE. Neural substrates of fluid reasoning: an fMRI study of neocortical activation during performance of the Raven's progressive matrices test. *Cogn Psychol*. 1997:33(1):43–63. https://doi.org/10.1006/cogp.1997.0659.

Raudies F, Hasselmo ME. A model of symbolic processing in Raven's progressive matrices. *Biol Inspired Cogn Archit*. 2017:21:47–58. https://doi.org/10.1016/j.bica.2017.07.003.

Raven JC. Standardization of progressive matrices. *Br J Med Psychol*. 1941:19(1):137–150. https://doi.org/10.1111/j.2044-8341.1941.tb00316.x.

Ray KL, Ragland JD, MacDonald AW, Gold JM, Silverstein SM, Barch DM, Carter CS. Dynamic reorganization of the frontal parietal network during cognitive control and

episodic memory. *Cogn Affect Behav Neurosci*. 2020:20(1):76–90. https://doi.org/10.3758/S13415-019-00753-9/FIGURES/6.

Rosvall M, Bergstrom CT. Mapping change in large networks. *PLoS One*. 2010:5(1):e8694. https://doi.org/10.1371/JOURNAL.PONE.0008694.

Rubinov M, Sporns O. Complex network measures of brain connectivity: uses and interpretations. *NeuroImage*. 2010:52(3):1059–1069. https://doi.org/10.1016/J.NEUROIMAGE.2009.10.003.

Rubinov M, Sporns O. Weight-conserving characterization of complex functional brain networks. *NeuroImage*. 2011:56(4):2068–2079. https://doi.org/10.1016/j.neuroimage.2011.03.069.

Sahyoun CP, Belliveau JW, Soulières I, Schwartz S, Mody M. Neuroimaging of the functional and structural networks underlying visuospatial vs. linguistic reasoning in high-functioning autism. *Neuropsychologia*. 2010:48(1):86–95. https://doi.org/10.1016/j.neuropsychologia.2009.08.013.

Salvo JJ, Holubecki AM, Braga RM. Correspondence between functional connectivity and task-related activity patterns within the individual. *Curr Opin Behav Sci*. 2021:40:178–188. https://doi.org/10.1016/J.COBEHA.2021.05.003.

Schaefer A, Kong R, Gordon EM, Laumann TO, Zuo X-N, Holmes AJ, Eickhoff SB, Yeo BTT. Local-Global Parcellation of the Human Cerebral Cortex from Intrinsic Functional Connectivity MRI. *Cerebral Cortex*. 2017:28(9):3095–3114. https://doi.org/10.1093/cercor/bhx179.

Scheid BH, Ashourvan A, Stiso J, Davis KA, Mikhail F, Pasqualetti F, Litt B, Bassett DS. Time-evolving controllability of effective connectivity networks during seizure progression. *Proc Natl Acad Sci U S A*. 2021:118(5):2006436118. https://doi.org/10.1073/PNAS.2006436118/-/DCSUPPLEMENTAL.

Schendan HE, Stern CE. Mental rotation and object categorization share a common network of prefrontal and dorsal and ventral regions of posterior cortex. *NeuroImage*. 2007:35(3):1264–1277. https://doi.org/10.1016/J.NEUROIMAGE.2007.01.012.

Schendan HE, Stern CE. Where vision meets memory: prefrontal–posterior networks for visual object constancy during categorization and recognition. *Cereb Cortex*. 2008:18(7):1695–1711. https://doi.org/10.1093/cercor/bhm197.

Schultz DH, Cole XW. Higher intelligence is associated with less task-related brain network reconfiguration. *J Neurosci*. 2016:36(33):8551–8561. https://doi.org/10.1523/JNEUROSCI.0358-16.2016.

Setsompop K, Gagoski BA, Polimeni JR, Witzel T, Wedeen VJ, Wald LL. Blipped-controlled aliasing in parallel imaging for simultaneous multislice echo planar imaging with reduced g-factor penalty. *Magn Reson Med*. 2012:67:1210–1224.

Shin M, Jeon H-A. A cortical surface-based meta-analysis of human reasoning. *Cereb Cortex*. 2021:31(12):5497–5510. https://doi.org/10.1093/CERCOR/BHAB174.

Sloman SA, Lagnado DA. The Problem of Induction. In: Holyoak KJ, Morrison RG, editors. *The Cambridge handbook of thinking and reasoning*. Cambridge University Press; 2005. pp. 95–116.

Sokolowski HM, Fias W, Mousa A, Ansari D. Common and distinct brain regions in both parietal and frontal cortex support symbolic and nonsymbolic number processing in humans: a functional neuroimaging meta-analysis. *NeuroImage*. 2017:146:376–394. https://doi.org/10.1016/J.NEUROIMAGE.2016.10.028.

Thiele JA, Faskowitz J, Sporns O, Hilger K. Multitask brain network reconfiguration is inversely associated with human intelligence. *Cereb Cortex*. 2021:32(19):4172–4182. https://doi.org/10.1093/CERCOR/BHAB473.

Tobyne SM, Somers DC, Brissenden JA, Michalka SW, Noyce AL, Osher DE. Prediction of individualized task activation in sensory modality-selective frontal cortex with connectome fingerprinting. *NeuroImage*. 2018:183:173–185. https://doi.org/10.1016/j.neuroimage.2018.08.007.

Tomasi D, Volkow ND. Association between brain activation and functional connectivity. *Cereb Cortex*. 2019:29(5):1984–1996. https://doi.org/10.1093/CERCOR/BHY077.

Vakhtin AA, Ryman SG, Flores RA, Jung RE. Functional brain networks contributing to the Parieto-Frontal Integration theory of intelligence. *NeuroImage*. 2014:103:349–354. https://doi.org/10.1016/J.NEUROIMAGE.2014.09.055.

van den Heuvel MP, Sporns O. Rich-club organization of the human connectome. *J Neurosci*. 2011:31(44):15775–15786. https://doi.org/10.1523/JNEUROSCI.3539-11.2011.

van der Kouwe AJW, Benner T, Salat DH, Fischl B. Brain morphometry with multiecho MPRAGE. *NeuroImage*. 2008:40(2):559–569. https://doi.org/10.1016/j.neuroimage.2007.12.025.

Van Opstal F, Verguts T. Is there a generalized magnitude system in the brain? Behavioral, neuroimaging, and computational evidence. *Front Psychol*. 2013:4:435. https://doi.org/10.3389/fpsyg.2013.00435.

Wallis JD, Anderson KC, Miller EK. Single neurons in prefrontal cortex encode abstract rules. *Nature*. 2001:411(6840):953–956. https://doi.org/10.1038/35082081.

Walsh V. A theory of magnitude: common cortical metrics of time, space and quantity. *Trends Cogn Sci*. 2003:7(11):483–488. https://doi.org/10.1016/J.TICS.2003.09.002.

Watson CE, Chatterjee A. A bilateral frontoparietal network underlies visuospatial analogical reasoning. *NeuroImage*. 2012:59(3):2831–2838. https://doi.org/10.1016/J.NEUROIMAGE.2011.09.030.

Wendelken C, Chung D, Bunge SA. Rostrolateral prefrontal cortex: domain-general or domain-sensitive? *Hum Brain Mapp*. 2012:33(8):1952–1963. https://doi.org/10.1002/hbm.21336.

Whitfield-Gabrieli S, Nieto-Castanon A. Conn: a functional connectivity toolbox for correlated and anticorrelated brain networks. *Brain Connect*. 2012:2(3):125–141. https://doi.org/10.1089/BRAIN.2012.0073.

Xu J, Moeller S, Auerbach EJ, Strupp J, Smith SM, Feinberg DA, Yacoub E, Ugurbil K. Evaluation of slice accelerations using multiband echo planar imaging at 3 T. *NeuroImage*. 2013:83:991–1001.

Yeo BTT, Krienen FM, Sepulcre J, Sabuncu MR, Lashkari D, Hollinshead M, Roffman JL, Smoller JW, Zöllei L, Polimeni JR, et al. The organization of the human cerebral cortex estimated by intrinsic functional connectivity. *J Neurophysiol*. 2011:106(3):1125–1165. https://doi.org/10.1152/jn.00338.2011.

Zhang Y, Brady M, Smith S. Segmentation of brain MR images through a hidden Markov random field model and the expectation-maximization algorithm. *IEEE Trans Med Imaging*. 2001:20(1):45–57. https://doi.org/10.1109/42.906424.

Zhou D, Cornblath EJ, Stiso J, Teich EG, Dworkin JD, Blevins AS, Bassett DS. Gender diversity statement and code notebook v1.0. *Zenodo*. 2020. https://doi.org/10.5281/zenodo.3672110.

Zhu H, Paschalidis IC, Chang A, Stern CE, Hasselmo ME. A neural circuit model for a contextual association task inspired by recommender systems. *Hippocampus*. 2020:30(4):384–395. https://doi.org/10.1002/hipo.23194.